NANO LETTERS

2007
Vol. 7, No. 9
2881−2885

Separation of Nanoparticles by Gel Electrophoresis According to Size and Shape

Matthias Hanauer, Sebastien Pierrat, Inga Zins, Alexander Lotz, and Carsten Sönnichsen*

Institute for Physical Chemistry, University of Mainz, Jakob-Welder-Weg 11, 55128 Mainz, Germany

Received July 5, 2007; Revised Manuscript Received August 4, 2007

ABSTRACT

We demonstrate the separation of gold and silver nanoparticles according to their size and shape by agarose gel electrophoresis after coating them with a charged polymer layer. The separation is monitored optically using the size- and shape-dependent plasmon resonance of noble metal particles and confirmed by transmission electron microscopy (TEM). Electrophoretic mobilities are quantitatively explained by a model based on the Henry formula, providing a theoretical framework for predicting gel mobilities of polymer coated nanoparticles.

The chemical synthesis of inorganic nanoparticles in solution often yields a large distribution of particle sizes and multiple particle shapes, e.g., rods, spheres, and triangles.[1−5] To use size- and/or shape-dependent material properties, such as quantum confinement or plasmon resonances, it is critical to have nanoparticles with the lowest size and shape dispersion possible. The need for ultranarrow size and shape distributions becomes highly important for self-assembly of nanoparticles over large areas, which would be required for many devices, for example, solar cells.[6,7] An alternative to the high-yield synthesis of nanoparticles with ultranarrow size distribution is the postsynthetic separation of particles similar to cleaning procedures in organic synthesis.

We show here how the technique of gel electrophoresis is successfully used to separate nanoparticles according to size and shape. Gel electrophoresis is commonly used to separate biomolecules[8−10] and has been used to sort nanoparticles according to the exact number of attached polymer chains.[11−15] We separate polymer-coated spherical, rod-shaped, and triangular gold and silver nanoparticles, which show strong colors induced by plasmon resonances. The strong influence of size and shape on the frequency or wavelength of the plasmon resonance would make it desirable to obtain monodisperse samples for optical applications.[16] The strong shape/color relationship also allows direct visual or spectroscopic analysis of successful separations, which appear as multicolored lanes in a gel. Compared to other separation techniques such as centrifugation, high-performance liquid chromatography (HPLC),[17] capillary electrophoresis,[18] diafiltration,[19] or size-exclusion chromatography,[20] gel electrophoresis has the advantage of allowing multiple runs in parallel on the same gel, which is a considerable advantage at the stage of understanding mechanisms and optimizing conditions.

We prepare gold and silver nanorod samples using the seeded growth technique[21−23] as described in the Supporting Information. It is possible to prepare gold nanorods in high yield (>95%) and with relatively small size deviations (≈ 10% variation in aspect ratio). Silver nanorods, however, only represent a small subpopulation of the synthesized particles and there is currently no simple and reliable method to produce them as purely as the gold rods. Figure 1a shows a typical transmission electron microscopy (TEM) image of a silver sample with 13% rods, 34% spheres (including hexagons), 44% triangles, and 9% other shapes (established from counting 600 particles, details in Supporting Information, Figure S1). To stabilize the nanoparticles, we coat them with a layer of polyethylene glycol (PEG, MW 5000), which is covalently attached at one end to the metal surface via a thiol group ("PEGylation"). The other end of the polymer chain may carry different functional groups, which we exploit for controlling the overall particle charge and mobility.[24] In the following we use SH-PEG-COOH. After PEGylation, we run the silver sample in an 0.2% agarose gel in 0.5× TBE (Tris-borate EDTA) buffer (pH ≈ 9) together with gold spheres and gold rods (Figure 1b, true color photograph, no staining; details of the preparation methods are given in the Supporting Information). The gel shows different colors in the silver lane and clear separation of gold spheres (red)

* Corresponding author. E-mail: soennichsen@uni-mainz.de. Fax: +49 6131 3926747. Web address: http://www.nano-bio-tech.de.

10.1021/nl071615y CCC: $37.00
Published on Web 08/24/2007

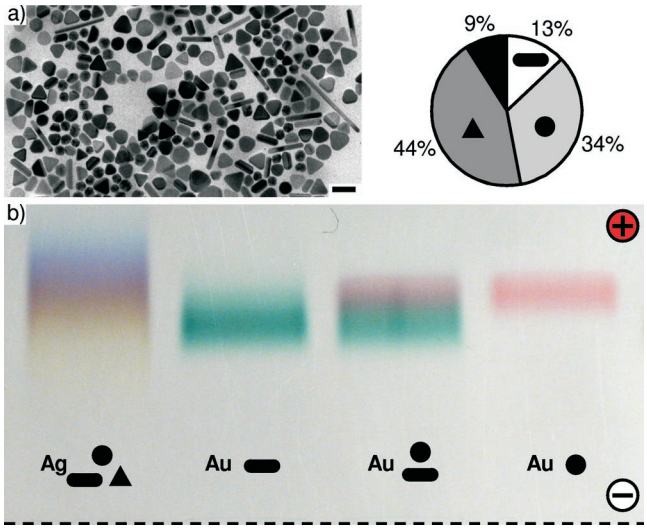

Figure 1. (a) Typical TEM picture of a silver nanoparticle sample (left, scale bar 100 nm) and the proportion of spheres, triangles, and rods (right) analyzed by assigning shapes to 600 particles by eye. (b) True color photograph of a 0.2% agarose gel run for 30 min at 150 V (15 cm electrode spacing) in 0.5× TBE buffer (pH ≈ 9). The dashed line at the bottom indicates the position of the gel wells. The four lanes contain, from left to right, silver nanoparticles, gold nanorods (≈ 40 × 20 nm), gold rods and spheres mixed just before electrophoresis, and spherical gold nanoparticles (∅ ≈ 15 nm) as indicated symbolically. All nanoparticles are stabilized by a coating of 100% SH-PEG-COOH. The colors are due to the size- and shape-dependent optical properties of gold and silver particles and indicate separation according to nanoparticle morphology.

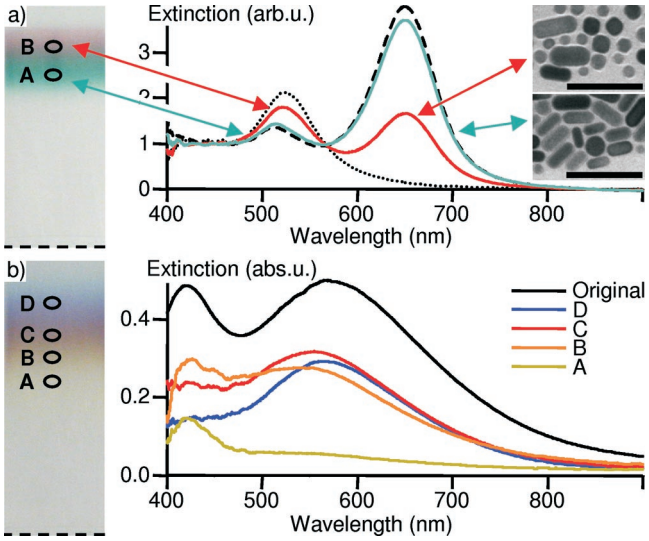

Figure 2. (a) Separation of gold nanospheres and rods. Normalized extinction spectra of spots in the gel as indicated on the left and TEM images of samples collected at those positions (insets, scale bars 100 nm). Fraction A shows a higher extinction at 650 nm compared to fraction B. The dashed line is the spectrum of the pure gold rods sample (lane 2, Figure 1b), the dotted line corresponds to the pure gold spheres sample (lane 4, Figure 1b). Quantitative analysis of the extinction values at 520 and 650 nm leads to a high percentage of rods in fraction A (69%) in contrast to fraction B (12%). Counting the particles on the TEM pictures leads to the same results (72% and 11%, respectively). (b) Extinction spectra of the fractions A, B, C, and D show a separation of silver nanoparticles by shape because the peak at 580 nm increases and the peak at 420 nm decreases. Because the characteristic resonance wavelength of silver rods is not well-known and may coincide with triangle plasmons, the quantification of extinction values is not meaningful for silver particles.

mixed with gold rods (green). This is a visual proof for successful separation of nanoparticles.

We analyze the particle distribution in the various regions of the gel by two methods: local extinction spectroscopy and TEM. Local extinction spectra are taken by focusing the light from a fiber-coupled tungsten light source (Ocean Optics, FL-2000-FHSA) to a spot of about 1 mm^2 and recording the transmitted light with a fiber spectrometer (Ocean Optics, USB2000). The resulting spectra for the indicated locations on the gel are shown in Figure 2a (gold) and b (silver). The gold rods have two extinction maxima according to the plasmon resonance of their long axis (≈ 650 nm) and short axis (≈ 520 nm), the latter coinciding with the extinction maximum of the spherical particles. The intensities at those two wavelengths allow one to estimate the particle concentrations from tabulated extinction coefficients[25,26] ($\varepsilon_{spheres,520\ nm} = 0.344$/nmol cm, $\varepsilon_{rods,650\ nm} = 3.00$/nmol cm, details in the Supporting Information) and show a change in the percentage of rods from 69% to 12% between the two fractions (compared to 25% in the original sample). For the silver particles, such a simple optical estimation of the separation efficiency is not possible due to the lack of pure controls for triangles and rods. However, the mobility of silver and gold spheres of the same size are comparable (Supporting Information, Figure S2a).

To verify the results of the optical spectra for gold nanoparticles and to get results for the silver particles, we use transmission electron microscopy. Conventional carbon-coated copper TEM grids were inserted at the places indicated (Figure 2) after cutting the gel gently with a surgical knife. By running the gel for another 3 min, particles deposit on the grids. After drying, they were inspected in a transmission electron microscope operating at 120 kV (Phillips CM12). The size and the shape of all particles on the images was measured (250−650 particles per fraction). Typical images of gold particles are shown in the inset in Figure 2a. Counting spheres and rods on the TEM pictures leads to a percentage of rods of 72% in the first fraction and 11% in the second. Those values agree well with the values determined optically and thus confirm the accuracy of the TEM method.[27] The separation is not perfect yet, which is most likely caused by a variation in the number of charges per particle and the small overall particle charge.

After having established the reliability of the analysis method, the inhomogeneous silver sample was analyzed with the TEM method. Figure 3a shows representative TEM images obtained from the indicated positions in the gel. For each of these four locations, we counted about 100 particles and classified them according to shape as rods, spheres, and triangles. Figure 3b shows their percentages at the four locations and compares them with their proportions in the original sample. Rods are predominantly located in the fraction containing the particles with the lowest mobility,

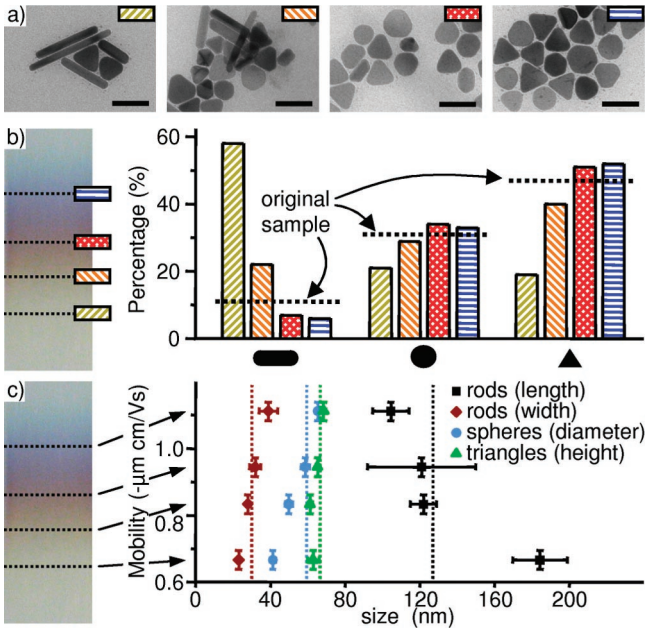

Figure 3. (a) Typical TEM images obtained from different parts of the gel lane containing silver nanoparticles (lane 1, Figure 1b). The positions are indicated using a color code (scale bars 100 nm). (b) Detailed statistics of the qualitative sample composition in terms of rods, spheres, and triangles at the four positions (460 particles counted). The first set of bars, for example, shows that silver rods are predominantly found in the slowest moving fraction, where they account for 60% of the particles as compared to only 7% in the fastest fraction. (c) Careful quantitative analysis shows a separation of particles according to sphere diameter and rod aspect ratio. The average sphere diameter increases from 41 ± 2 nm in the slowest fraction to 65 ± 2 nm in the fastest fraction. The aspect ratio (length/width) of silver rods decreases from 8.3 ± 0.8 to 3.1 ± 0.7. For the triangles, we observe no influence of the height on the mobility. The vertical lines indicate the mean sizes in the original sample (Supporting Information, Figure S1).

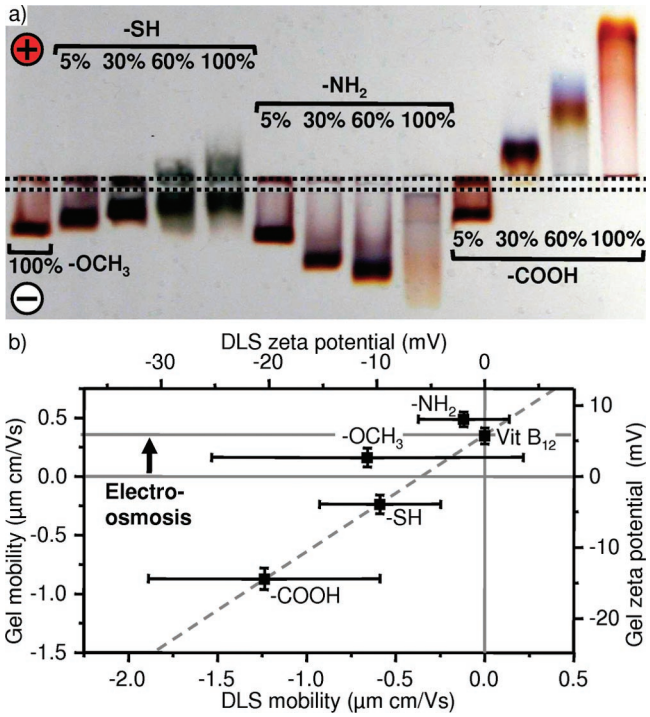

Figure 4. (a) Electrophoretic separation of silver nanoparticles according to surface coating in a 0.3% agarose gel run for 30 min at 150 V (15 cm electrode spacing) in 0.5× TBE buffer (pH ≈ 9). The coating consists of SH-PEG-X molecules with −X = $-OCH_3$, −SH, $-NH_2$, or −COOH as indicated. The different fractions are prepared by mixing different proportions of SH-PEG-X with SH-PEG-OCH_3. The two horizontal lines mark the position of the gel wells. −SH-functionalized particles are retarded compared to the $-OCH_3$ reference, which moves slightly toward the negative electrode. The $-NH_2$ functionalized particles move faster toward the negative electrode with increasing $-NH_2$ fraction, while the −COOH functionalized ones move clearly to the positive electrode and show a separation into different colors. (b) Comparison of the mobilities of gold spheres (∅ ≈ 20 nm, BBI), deduced from analyzing gels with those measured by dynamic light scattering (DLS). The ζ potential is calculated from the measured mobilities using the Henry formula. Those mobilities agree within the errors of the experiments, except for an offset caused by electro-osmotic flow in the gel as shown by the mobility of vitamin B_{12}.

where their percentage is increased from 13% in the original sample to 60%. Spheres show a slight tendency to accumulate in the faster fractions. The triangles are clearly enriched in the fastest moving fraction (50% in the fastest vs 20% in the slowest).

A more quantitative result is obtained by measuring the length of the long and short axis for the rods, the diameter for spheres, and the height for triangles. The electrophoretic mobility is shown in Figure 3c as a function of those parameters (mean values with standard error). The nanorods with the highest aspect ratio clearly move the slowest: the average aspect ratio of rods is 8.3 ± 0.8 in the slowest fraction, whereas it is 3.1 ± 0.7 in the fastest one. For the spherical particles, we find a clear trend of increasing mobility with increasing size: the average diameter of the spheres increases from 41 ± 2 to 65 ± 2 nm from the slowest to the fastest fraction. The mobility of the triangles shows no clear trend. Because the triangles are probably flat[28] and their thickness cannot be determined from our TEM images, the mobility may be influenced by this hidden parameter. The fact that the observed sizes averaged over all fractions agree well with the mean sizes of the triangles, spheres, and rods measured on the original sample (Supporting Information, Figure S1 and vertical lines in Figure 3c) shows again the reliability of the sampling and the self-consistency of the results.

So far we have discussed negatively charged nanoparticles coated by a layer of SH-PEG-COOH because the −COOH group is deprotonated in the basic environment of the TBE buffer (pH ≈ 9). We find that this coating gives the best separation of silver nanorods, as judged from the appearance of a multicolored lane. Using $-OCH_3$, −SH, or $-NH_2$ as functional groups or mixing them with $-OCH_3$ in various proportions leads to a less-pronounced separation (Figure 4a). The $-OCH_3$ functionalized nanorods move slightly to the negative electrode, the −SH functionalized nanoparticles as well, but with decreasing speed as the percentage of −SH increases. The $-NH_2$ functionalized nanorods move strongly toward the negative electrode and the mobility increases with $-NH_2$ percentage. The lane for 100% $-NH_2$ coating shows some smearing out, which is, however, not always reproducible and probably due to some aggregation or interactions

between the positively charged particles and the negatively charged gel matrix.[10]

For gold spheres ($\varnothing \approx 20$ nm, British Biocell International, BBI) carrying the four types of end groups, we compare the electrophoretic mobilities measured in agarose gels with values determined by dynamic light scattering (DLS, using a Zeta Sizer Nano ZS90, Malvern Instruments).[29,30] The results show reasonable agreement within the errors (Figure 4b). There is an offset in the gel values caused by electro-osmosis (EEO),[31] which we estimate independently by running vitamin B_{12} (Supporting Information, Figure S2). Vitamin B_{12} is known to run mainly by electro-osmosis in our conditions, and the value of $\mu_{EEO} \approx 0.315$ μm cm/Vs obtained is in agreement with a previous report.[32] The magnitude of the measured electro-osmosis effect μ_{EEO} corresponds[33] to a surface potential of the agarose gel of $\zeta_{gel} = -4$ mV, using $\mu_{EEO} = -\varepsilon\zeta/\eta$ with the dielectric constant ε and the viscosity η of the solvent (here $\varepsilon = 81\ \varepsilon_0$ and $\eta = 0.89$ cP at 25 °C).[34] Such a negative value for the potential of the gel walls is plausible.[10] In the following, all mobility values are corrected for the electro-osmotic effect.

The mobility μ_E of a charged colloid with radius a can be calculated from the zeta potential ζ using the Henry formula[33] $\mu_E = (2\varepsilon\zeta/3\eta)\, f_1(\kappa a)$, where f_1 is a correction factor given by $f_1(\kappa a) = 1 + 1/(2(1 + \delta/\kappa a)^3)$ with $\delta = 2.5/(1 + 2e^{-\kappa a})$. In these equations, $1/\kappa$ is the Debye length. In our case (0.5× TBE buffer, ionic strength 0.02 mol/L), the Debye length is $1/\kappa = 2.1$ nm. For a particle with a diameter of $2a = 20$ nm, κa is about 5 and $f_1 = 1.14$. Note that, in the Hückel limit ($\kappa a \ll 1$) $f_1 = 1$, in the Smoluchowski-approximation ($\kappa a \gg 1$) $f_1 = 1.5$, so neither may be used here with confidence. The ζ potentials calculated by the Henry formula given above are shown on the second axis in Figure 4b and give values of about −17 to +5 mV, which are sufficiently low to neglect the high-potential corrections to the Henry formula. If we use the Henry model, we can explain the sign and the magnitude of the observed mobilities. From the Gouy−Chapman formula,[33] $\sigma = \varepsilon\zeta\,(1 + 1/\kappa a)$, we estimate the ζ potential using a constant surface charge density σ. Together with the Henry model, the resulting radius dependency of the mobilities is not sufficient to explain the observed separation of silver spheres in Figure 3c. Using σ derived from the mobility of the medium particle fraction ($\varnothing \approx 50$ nm), the calculation yields a retardation of 11% of the small particle fraction ($\varnothing \approx 41$ nm) relative to the large particle fraction ($\varnothing \approx 65$ nm), whereas the measured retardation is about 40%. However, the PEG layer adds to the hydrodynamic radius, enhancing the retardation effect, especially for smaller particles. Therefore, we have to replace the parameter a with the effective particle radius $a + R$ including the thickness R of the PEG layer. For simplicity, we fix the value for the density of charged PEG molecules on the particle surface (at radius a), i.e., ignoring the effect of surface curvature on the packing density of PEG. The latter is significant for particle radii similar to or smaller than the PEG layer thickness. We estimate R by comparing the hydrodynamic radius of PEG-coated gold spheres ($2a = 20$ nm) measured with DLS to the true particle radius a and find $R = 12.5$ nm. This experimental value is slightly bigger than the Flory radius $R_F = N^{0.64}\, b = 7.3$ nm (with $N = 114$, the number of PEG monomers, and $b = 0.35$ nm, the size of the monomer unit)[35] and significantly smaller than the extended chain length $l = Nb = 40$ nm. The PEG molecules are therefore slightly extended from their maximum entropy configuration but far from being completely stretched. We use the Henry model with the modified radius $a + R$ to explain the separation observed for silver spheres in Figure 3c. From the mobility −1.148 μm cm/Vs of the medium fraction of silver spheres ($2a = 50$ nm), which is corrected for the electro-osmotic effect (+0.315 μm cm/Vs), we obtain a density of 8 charged PEG molecules per 100 nm^2 on the particle surface. Using this value, we calculate mobilities of $\mu_E(2a = 41\text{ nm}) = -0.66$ μm cm/Vs to $\mu_E(2a = 65\text{ nm}) = -1.07$ μm cm/Vs, i.e., a retardation of 40% for the smallest particle fraction compared to the largest particles in Figure 3b, which is in agreement with the measured retardation of 40%.

As the mobility of particles in a gel is strongly depending on the surface charge density, it would be interesting to compare the PEG packing density for particles of different sizes. From the corrected mobility of SH-PEG-COOH coated gold spheres ($2a = 20$ nm, Figure 4b), we find a density of charged PEG molecules of 17 per 100 nm^2. Because a saturation of the mobility is observed when the proportion of SH-PEG-COOH to SH-PEG-OCH_3 is greater than 75% (Supporting Information, Figure S3, probably due to proximity effects), the overall density of attached PEG molecules is estimated to be about 23 per 100 nm^2. This value is higher than the value of 3−7 PEG molecules per 100 nm^2 reported earlier for gold nanorods[24] and compared to the silver spheres found above. Qualitatively, such a difference is plausible considering the surface curvature effect.[36]

The Henry formula, corrected for the thickness of the PEG layer, allows us to interpret qualitatively and quantitatively the measured mobilities without taking into account any gel matrix effects (except the offset caused by electro-osmosis). This seems justified by the fact that we are using very low agarose gel concentrations (<0.5%) giving pore diameters in the gel ($\varnothing = 200$−400 nm),[37] considerably larger than the size of the spherical particles. In support of this argument, we find that higher gel concentrations lead to worse separation (Supporting Information, Figure S4), probably due to increased particle/matrix interactions. These interactions result in temporary attachment of particles on the surface of the pores and hence in retardation of the fastest particles. The enrichment of long aspect ratio rods in the slowest moving fraction is caused, however, by the retardation effect of the gel. Hence, there is a delicate balance between pore size, particle charges, and electric field, resulting in a nice separation only for the narrow window of conditions we report here.

We are working on upscaling the separation process to larger quantities of particles necessary for many experiments and applications. The gel column currently used for this purpose (BIORAD model 491 Prep Cell) is afflicted with technical difficulties (e.g., the low gel concentration causes

handling problems). Preliminary results show that 65% of a mix of spherical[38] and rod-shaped particles inserted are recovered in different fractions, which show a clear separation of the particles according to their shape (Supporting Information, Figure S5).

In conclusion, we have shown the ability to separate silver particles according to their size and shape using gel electrophoresis. The measured particle mobilities are explained quantitatively using the Henry formula and the Gouy−Chapman model. We find values for the charge density of PEG coated gold and silver nanoparticles, the number of attached PEG molecules per surface area, the PEG layer thickness, and the gel surface potential. The ability to separate nanoparticles according to size and shape is an important step toward their use in devices and necessary for many studies of their fundamental properties.

Acknowledgment. We thank Prof. Dr. Manfred Schmidt and Nils Heimann for help with large-scale gel electrophoresis, Prof. Dr. Florian Banhart for help with electron microscopy, and we acknowledge financial support by the DFG under the Emmy Noether program.

Supporting Information Available: Figures showing the composition of the silver nanoparticle sample, the mobility of gold and silver spheres (BBI) coated with different SH-PEG-X, the mobility of silver particles as a function of the fraction of SH-PEG-COOH, the influence of gel concentration on separation efficiency, and preliminary results on upscaling the separation with a vertical column. Also details of the experimental procedures for particle synthesis, surface coating, gel preparation and analysis, dynamic light scattering, and details of the estimation of particle concentrations in the gel. This material is available free of charge via the Internet at http://pubs.acs.org.

References

(1) Perez-Juste, J.; Pastoriza-Santos, I.; Liz-Marzan, L. M.; Mulvaney, P. *Coord. Chem. Rev.* **2005**, *249*, 1870−1901.
(2) Eustis, S.; El-Sayed, M. A. *Chem. Soc. Rev.* **2006**, *35*, 209−217.
(3) Pileni, M. P. *Langmuir* **1997**, *13*, 3266−3276.
(4) Chen, H. M.; Peng, H. C.; Liu, R. S.; Asakura, K.; Lee, C. L.; Lee, J. F.; Hu, S. F. *J. Phys. Chem. B* **2005**, *109*, 19553−19555.
(5) Murphy, C. J.; Sau, T. K.; Gole, A. M.; Orendorff, C. J.; Gao, J.; Gou, L.; Hunyadi, S. E.; Li, T. *J. Phys. Chem. B* **2005**, *109*, 13857−13870.
(6) Manna, L. *Nano Lett.* **2007**, *7*, nl0717661.
(7) Milliron, D. J.; Hughes, S. M.; Cui, Y.; Manna, L.; Li, J. B.; Wang, L. W.; Alivisatos, A. P. *Nature* **2004**, *430*, 190−195.
(8) Viovy, J. L. *Rev. Mod. Phys.* **2000**, *72*, 813−872.
(9) Tietz, D. *J. Chromatogr.* **1987**, *418*, 305−344.
(10) Serwer, P. *Electrophoresis* **1983**, *4*, 375−382.
(11) Claridge, S. A.; Goh, S. L.; Frechet, J. M. J.; Williams, S. C.; Micheel, C. M.; Alivisatos, A. P. *Chem. Mater.* **2005**, *17*, 1628−1635.
(12) Parak, W. J.; Pellegrino, T.; Micheel, C. M.; Gerion, D.; Williams, S. C.; Alivisatos, A. P. *Nano Lett.* **2003**, *3*, 33−36.
(13) Zanchet, D.; Micheel, C. M.; Parak, W. J.; Gerion, D.; Williams, S. C.; Alivisatos, A. P. *J. Phys. Chem. B* **2002**, *106*, 11758−11763.
(14) Zanchet, D.; Micheel, C. M.; Parak, W. J.; Gerion, D.; Alivisatos, A. P. *Nano Lett.* **2001**, *1*, 32−35.
(15) Sperling, R. A.; Pellegrino, T.; Li, J. K.; Chang, W. H.; Parak, W. J. *Adv. Funct. Mater.* **2006**, *16*, 943−948.
(16) Sönnichsen, C.; Reinhard, B. M.; Liphardt, J.; Alivisatos, A. P. *Nat. Biotechnol.* **2005**, *23*, 741−745.
(17) Henglein, A. *J. Phys. Chem.* **1993**, *97*, 5457−5471.
(18) Liu, F. K.; Wei, G. T. *Anal. Chim. Acta* **2004**, *510*, 77−83.
(19) Sweeney, S. F.; Woehrle, G. H.; Hutchison, J. E. *J. Am. Chem. Soc.* **2006**, *128*, 3190−3197.
(20) Wei, G. T.; Liu, F. K.; Wang, C. R. C. *Anal. Chem.* **1999**, *71*, 2085−2091.
(21) Nikoobakht, B.; El-Sayed, M. A. *Chem. Mater.* **2003**, *15*, 1957−1962.
(22) Jana, N. R.; Gearheart, L.; Murphy, C. J. *Chem. Commun.* **2001**, 617−618.
(23) Jana, N. R.; Gearheart, L.; Murphy, C. J. *Adv. Mater.* **2001**, *13*, 1389−1393.
(24) Pierrat, S.; Zins, I.; Breivogel, A.; Sönnichsen, C. *Nano Lett.* **2007**, *7*, 259−263.
(25) Orendorff, C. J.; Murphy, C. J. *J. Phys. Chem. B* **2006**, *110*, 3990−3994.
(26) BBInternational: http://www.bbigold.com/.
(27) Counting particles on TEM images relies on representative sampling, which needs to be checked independently.
(28) Tao, A.; Sinsermsuksakul, P.; Yang, P. D. *Angew. Chem., Int. Ed.* **2006**, *45*, 4597−4601.
(29) Niidome, T.; Yamagata, M.; Okamoto, Y.; Akiyama, Y.; Takahashi, H.; Kawano, T.; Katayama, Y.; Niidome, Y. *J. Controlled Release* **2006**, *114*, 343−347.
(30) Pramod, P.; Joseph, S. T. S.; Thomas, K. G. *J. Am. Chem. Soc.* **2007**, *129*, 6712−6713.
(31) Ghosh, S.; Moss, D. B. *Anal. Biochem.* **1974**, *62*, 365−370.
(32) Serwer, P.; Hayes, S. J. *Electrophoresis* **1982**, *3*, 80−85.
(33) Hunter, R. J., *Foundations of Colloid Science*; Oxford University Press: New York, 2001.
(34) *CRC Handbook of Chemistry and Physics*, 85th ed.; CRC Press: Boca Raton, FL, 2004.
(35) Jeppesen, C.; Wong, J. Y.; Kuhl, T. L.; Israelachvili, J. N.; Mullah, N.; Zalipsky, S.; Marques, C. M. *Science* **2001**, *293*, 465−468.
(36) Ligoure, C.; Leibler, L. *Macromolecules* **1990**, *23*, 5044−5046.
(37) Griess, G. A.; Moreno, E. T.; Easom, R. A.; Serwer, P. *Biopolymers* **1989**, *28*, 1475−1484.
(38) Turkevich, J.; Stevenson, P. C.; Hillier, J. *Faraday Discuss.* **1951**, *11*, 55.

NL071615Y